Transient Inhibition of the JAK/STAT Pathway Prevents B-ALL Development in Genetically Predisposed Mice

Ana Casado-García[1,2], Marta Isidro-Hernández[1,2], Ninad Oak[3], Andrea Mayado[2,4], Christine Mann-Ran[5], Javier Raboso-Gallego[1,2], Silvia Alemán-Arteaga[1,2], Alexandra Buhles[5], Dario Sterker[5], Elena G. Sánchez[6], Jorge Martínez-Cano[7], Oscar Blanco[2,8], Alberto Orfao[2,4], Diego Alonso-López[9], Javier De Las Rivas[2,10], Susana Riesco[11], Pablo Prieto-Matos[2,11], África González-Murillo[6], Francisco Javier García Criado[2,12], María Begoña García Cenador[2,12], Thomas Radimerski[5], Manuel Ramírez-Orellana[6], César Cobaleda[7], Jun J. Yang[3,13], Carolina Vicente-Dueñas[2,11], Andreas Weiss[5], Kim E. Nichols[3], and Isidro Sánchez-García[1,2]

ABSTRACT

Preventing development of childhood B-cell acute lymphoblastic leukemia (B-ALL), a disease with devastating effects, is a longstanding and unsolved challenge. Heterozygous germline alterations in the *PAX5* gene can lead to B-ALL upon accumulation of secondary mutations affecting the JAK/STAT signaling pathway. Preclinical studies have shown that this malignant transformation occurs only under immune stress such as exposure to infectious pathogens. Here we show in $Pax5^{+/-}$ mice that transient, early-life administration of clinically relevant doses of ruxolitinib, a JAK1/2 inhibitor, significantly mitigates the risk of B-ALL following exposure to infection; 1 of 29 animals treated with ruxolitinib developed B-ALL versus 8 of 34 untreated mice. Ruxolitinib treatment preferentially targeted $Pax5^{+/-}$ versus wild-type B-cell progenitors and exerted unique effects on the $Pax5^{+/-}$ B-cell progenitor transcriptional program. These findings provide the first *in vivo* evidence for a potential strategy to prevent B-ALL development.

Significance: JAK/STAT inhibition suppresses tumorigenesis in a B-ALL–susceptible mouse model, presenting a novel approach to prevent B-ALL onset.

Introduction

B-cell acute lymphoblastic leukemia (B-ALL) is the most common childhood cancer and greatest cause of cancer-related death in children (1–3). For many types of childhood B-ALL, there exists a latent preleukemic phase in which the initiating somatic or germline genetic event is present, but leukemia does not develop. This clinically silent preleukemic condition is estimated to be present in more than 5% of the healthy childhood population and does not evolve to disease in the vast majority of cases (4). Several recent studies have provided strong evidence confirming the hypothesis that exposure to infections can be a driver of clonal evolution of preleukemic cells toward overt leukemia (5–11). It was thought for many years that activation-induced deaminase expression, which is upregulated in preleukemic B-cell precursors in response to infection, promoted secondary genetic changes leading to subsequent leukemia development (12). However, we now know that infection-mediated B-ALL does not result from expansion of a previously existing transformed clone or from random mutagenesis. Together, these findings suggest that B-ALL development might be preventable (13). Nevertheless, it has remained unclear how to target preleukemic B cells as a means to prevent the development of B-ALL.

Many approaches, including chemotherapy and pan-B cell antigen–targeting immunotherapies, have been remarkably successful in treating B-ALL. Although analogous targeting of preleukemic B cells could, in theory, help to prevent B-ALL development, the concomitant

[1]Experimental Therapeutics and Translational Oncology Program, Instituto de Biología Molecular y Celular del Cáncer, CSIC-USAL, Salamanca, Spain. [2]Institute of Biomedical Research of Salamanca (IBSAL), Salamanca, Spain. [3]Department of Oncology, St. Jude Children's Research Hospital, Memphis, Tennessee. [4]Servicio de Citometría, Departamento de Medicina, Biomedical Research Networking Centre on Cancer CIBER-CIBERONC (CB16/12/00400), Institute of Health Carlos III, and Instituto de Biología Molecular y Celular del Cáncer, CSIC/Universidad de Salamanca, Salamanca, Spain. [5]Novartis Institutes for BioMedical Research, Novartis Campus, Basel, Switzerland. [6]Department of Pediatric Hematology and Oncology, Hospital Infantil Universitario Niño Jesús, Universidad Autónoma de Madrid, Madrid, Spain. [7]Immune system development and function Unit, Centro de Biología Molecular Severo Ochoa (Consejo Superior de Investigaciones Científicas -Universidad Autónoma de Madrid), Madrid, Spain. [8]Departamento de Anatomía Patológica, Universidad de Salamanca, Salamanca, Spain. [9]Bioinformatics Unit, Cancer Research Center (CSIC-USAL), Salamanca, Spain. [10]Bioinformatics and Functional Genomics Research Group, Cancer Research Center (CSIC-USAL), Salamanca, Spain. [11]Department of Pediatrics, Hospital Universitario de Salamanca, Paseo de San Vicente, 58–182, Salamanca, Spain. [12]Departamento de Cirugía, Universidad de Salamanca, Salamanca, Spain. [13]Department of Pharmaceutical Sciences, St. Jude Children's Research Hospital, Memphis, Tennessee.

Note: Supplementary data for this article are available at Cancer Research Online (http://cancerres.aacrjournals.org/).

A. Casado-García, M. Isidro-Hernández, and N. Oak contributed equally as co-first authors and C. Vicente-Dueñas, A. Weiss, K.E. Nichols, and I. Sánchez-García as co-senior authors to this article.

Current address for T. Radimerski: Basilea Pharmaceutica, Basel, Switzerland.

Corresponding Authors: Isidro Sánchez-García, Experimental Therapeutics and Translational Oncology Program: Stem Cells, Cancer Stem Cells and Cancer, Instituto de Biología Molecular y Celular del Cáncer IBMCC, CSIC/Universidad de Salamanca, Campus M. de Unamuno S/N, Salamanca 37007, Spain. Phone: 349-2329-4813; E-mail: isg@usal.es; Carolina Vicente-Dueñas, cvd@usal.es; Andreas Weiss, andreas-2.weiss@novartis.com; and Kim E. Nichols, Kim.Nichols@STJUDE.ORG

Cancer Res 2022;82:1098–109

doi: 10.1158/0008-5472.CAN-21-3386

depletion of normal immune cells could result in severe and unacceptable immunosuppression in otherwise healthy children. Thus, therapies directed against preleukemic B cells require more selective targeting.

Germline mutations in the B-cell commitment gene *PAX5* confer susceptibility to B-ALL in humans that is characterized by the acquisition of cooperating somatic mutations in the JAK/STAT pathway (14–17). *Pax5*$^{+/-}$ mice faithfully mimic this genetic predisposition, and have demonstrated the critical role of exposure to a natural infectious environment in the evolution of the preleukemic clone to full-blown B-ALL (9, 13). This transformation is mediated by the appearance, in otherwise healthy *Pax5*$^{+/-}$ mice, of an aberrant IL7-sensitive progenitor compartment that is susceptible to malignant transformation through accumulation of secondary mutations in the JAK/STAT pathway on the basis of a selection pressure triggered by the exposure to delayed infection in conventional housing facilities (9). Consequently, we hypothesized that the presence of an IL7-sensitive immature B-cell population in *Pax5*$^{+/-}$ mice, which is sensitive to JAK inhibition *in vitro* (9), could constitute a therapeutic vulnerability of this pathway in *Pax5*$^{+/-}$ preleukemic cells. Thus, targeting the JAK/STAT pathway in *Pax5*$^{+/-}$ B cells could promote killing of preleukemic cells while preserving healthy B cells.

Here, we have addressed this hypothesis by demonstrating that transient oral administration of the JAK1/2 inhibitor ruxolitinib differentially targeted precursor B cells in *Pax5*$^{+/-}$ mice and resulted in prevention of B-ALL development under oncogenic environmental conditions. Thus, targeting the deregulated JAK/STAT pathway represents a novel and promising preventive strategy for this hereditary leukemia. As the presence of a precancerous cell is a common feature of many other forms of human leukemia as well as other cancers, our approach provides a general proof of principle for the development of similar preventive strategies for other cancer types, including those that do not rely on this pathway.

Materials and Methods

Data reporting

Sample sizes were determined on the basis of the literature describing mouse modeling of natural infection-driven leukemia (9) and were justified by power calculations estimating 90% power to detect differential leukemia incidence. The experiments were not randomized and the investigators were not blinded to allocation during experiments and outcome assessment.

Mouse model for natural infection-driven leukemia

Heterozygous *Pax5* mice (*Pax5*$^{+/-}$; ref. 18) and wild-type (WT) control mice were bred and maintained in the specific pathogen-free (SPF) area of the animal house until the moment when they were relocated to an environment where natural infectious agents were present, as described previously (9). All mouse experiments were performed following applicable Spanish and European legal regulations, and had been previously authorized by the pertinent institutional committees of both University of Salamanca (Salamanca, Spain) and Spanish Research Council (CSIC) under the approved project license (number: 607). The study includes both male and female mice. There were no mice excluded from any experimental group. Housing environmental conditions included a temperature of 21°C ±2°, humidity of 55% ±10%, and a 12-hour:12-hour light: dark cycle. Mice had access to food and water *ad libitum*. During housing, animals were monitored daily for health status. *Pax5*$^{+/-}$ and WT mice of a mixed C57BL/6×CBA background were used in this study. We used WT and *Pax5*$^{+/-}$ littermates of the same breeding to establish the control groups. When animals showed evidence of illness [lethargy, decreased appetite, and weight loss or detection of blast cells in peripheral blood (PB)], they were humanely euthanized, and organs were extracted by standard dissection. All major organs were macroscopically inspected under the stereo microscope and representative samples of tissue were cut and immediately fixed. Differences in Kaplan–Meier survival plots of transgenic mice and WT mice treated or not with ruxolitinib were analyzed using the log-rank (Mantel–Cox) test. Statistical analyses were performed by using GraphPad Prism v5.01 (GraphPad Software).

Generation of a targeted mouse line conditionally expressing *mJak3*^{V670A} in *Pax5*$^{+/-}$ precursor B cells

The *mJak3*^{V670A} cDNA was targeted to the ubiquitously expressed *Rosa26* locus (19) where the GFP (eGFP) was linked to the mouse *Jak3*^{V670A} cDNA via an internal ribosomal entry site. In the absence of Cre, neither *Jak3*^{V670A} nor *eGFP* is expressed. The *Rosa26-mJak3*^{V670A} mice were bred to *Mb1-Cre* (20) previously crossed with *Pax5*$^{+/-}$ mice (18) to generate *Rosa26-mJak3*^{V670A} + *Mb1-Cre* + *Pax5*$^{+/-}$ mice. Also *Rosa26-mJak3*^{V670A} + *Mb1-Cre* + *Pax5*$^{+/+}$ mice were generated as controls.

Preparation of ruxolitinib food pellets

For the pilot study, food pellets were prepared with ruxolitinib. Ruxolitinib content in pellets was 0.375 and 0.75 g/kg of food. Powdered food was mixed with water and ruxolitinib monophosphate (formulated as suspension in 0.5% methylcellulose), pressed into a cylindrical mold, cut into pellets and dried for 48 hours under high air flow at room temperature. Food pellets were provided *ad libitum* in the pellet rack of the animal cages at start of the experiment. For the 4-week study, food pellets without or with ruxolitinib (0.375 g/kg of food) were custom made at Profimi Kliba SA/Kliba Nafag (Switzerland).

Pilot pharmacokinetic study

Pax5$^{+/-}$ animals were fed with food pellets containing ruxolitinib at 0.375 and 0.75 g/kg of food *ad libitum* ($n = 5$/group) for 14 days. Blood samples were taken from animals 2 hours after start of the active dark phase (corresponding to C_{max}) and 2 hours prior end of the inactive light phase (corresponding to C_{min}), three times per week during the treatment period. Ruxolitinib levels were determined by LC/MS-MS method. Food consumption per cage was measured daily and back-calculated to an average food intake per mouse per day.

Flow cytometric analysis

Nucleated cells were obtained from total mouse bone marrow (BM; flushing from the long bones), PB, thymus, lymph nodes (LN), or spleen. Contaminating red blood cells were lysed with red cell lysis buffer and the remaining cells were washed in PBS with 1% FCS. After staining, all cells were washed once in PBS and were resuspended in PBS with 1% FCS containing 10 μg/mL propidium iodide (PI) to excluded dead cells from analyses and sorting procedures. The samples and the data were acquired in an AccuriC6 Flow Cytometer and analyzed using Flowjo software. Specific fluorescence of FITC, PE, PI, and APC excited at 488 nm (0.4 W) and 633 nm (30 mW), respectively, as well as known forward and orthogonal light scattering properties of mouse cells were used to establish gates. Nonspecific antibody binding was suppressed by preincubation of cells with CD16/CD32 Fc-block solution (BD Biosciences, catalog no. 553142). For each analysis, a total of at least 50,000 viable (PI) cells were assessed. The different immune cell populations were determined as follows: peripheral mature B cells ($B220^{+}IgM^{+/-}$), peripheral CD4 T cells ($CD4^{+}$ $CD8^{-}$), peripheral

CD8 T cells ($CD4^-$ $CD8^+$), peripheral granulocytes ($Gr1^{hi}$ $Mac1^{hi}$), BM pro-B and pre-B cells ($B220^{low}IgM^-$), BM pro-B cells ($CD19^+$c-Kit^+), BM pre-B cells ($B220^{low}CD25^+IgM^-$), BM recirculating B cells ($B220^{hi}IgM^{+/-}$), BM immature B cells ($B220^{low}IgM^+$), BM CD4 T cells ($CD4^+$ $CD8^-$), BM CD8 T cells ($CD4^-$ $CD8^+$), BM granulocytes ($Gr1^{hi}$ $Mac1^{hi}$), spleen and LNs mature B cells ($CD19^+B220^+$) and ($B220^+IgM^{+/-}$). The following antibodies were used for flow cytometry: anti-B220 (RA3-6B2, catalog no. 103212), CD4 (RM4–5, 1:250, catalog no. 100516), CD8a (53-6.7, 1:250, catalog no. 100708), CD11b/Mac1 (M1/70, 1:200, catalog no. 553310), CD19 (1D3, catalog no. 152404), CD117/c-Kit (2B8, 1:200, catalog no. 105807), Ly-6G/Gr1 (RB6-8C5; catalog no. 108412), IgM (R6-60.2, catalog no. 406509), and CD25 (PC61, catalog no. 553866) antibodies. All antibodies were purchased from BioLegend and used at a 1:100 dilutions unless otherwise indicated.

Quantification of serum cytokine levels

Serum cytokine levels were analyzed using the Cytometric Bead Array immunoassay system (BD Biosciences), which assesses simultaneously IL2, IL4, IL6, IL10, IL17A, TNFα, and IFNγ (Mouse Th1 Th2 Th17 Cytokine Kit #560485; BDB) and the IL1β assay (Mouse IL1β Enhanced Sensitivity Flex Set #562278; BDB). Briefly, 50 μL of the serum was incubated for 2 hours at room temperature with 50 μL of anticytokine MAb-coated beads and 50 μL of the appropriate PE-conjugated anticytokine antibody detector. After this incubation period, samples were washed once (5 minutes at 200 g) to remove the excess of detector antibodies. Immediately afterward, data acquisition was performed on a FACSCanto II flow cytometer (BDB) using the FACSDiva software program (BDB). During acquisition, information was stored for 3,000 events corresponding to each bead population analyzed per sample (total number of beads >9,000). For data analysis, FCAP Array Software v3.0 program (BDB) was used.

Histology

Tissue samples were formalin fixed and embedded in paraffin. Pathology assessment was performed on hematoxylin-eosin–stained sections under the supervision of O. Blanco, an expert pathologist at the Salamanca University Hospital.

V(D)J recombination

Immunoglobulin rearrangements were amplified by PCR using the primers below. Cycling conditions consisted of an initial heat activation at 95°C followed by 31–37 cycles of denaturation for 1 minute at 95°C, annealing for 1 minute at 65°C, and elongation for 1 minute 45 seconds at 72°C. This was followed by a final elongation for 10 minutes at 72°C. To determine the DNA sequences of individual V(D)J rearrangements, the PCR fragments were isolated from the agarose gel and cloned into the pGEM-Teasy vector (Promega); the DNA inserts of at least 10 clones corresponding to the same PCR fragment were then sequenced. The primers used for VDJ recombination analysis are listed in **Table 1**.

Table 1. List of primer pairs used for VDJ recombination analysis.

V_HJ558	forward	CGAGCTCTCCARCACAGCCTWCATGCARCTCARC
	reverse	GTCTAGATTCTCACAAGAGTCCGATAGACCCTGG
V_H7183	forward	CGGTACCAAGAASAMCCTGTWCCTGCAAATGASC
	reverse	GTCTAGATTCTCACAAGAGTCCGATAGACCCTGG
V_HQ52	forward	CGGTACCAGACTGARCATCASCAAGGACAAYTCC
	reverse	GTCTAGATTCTCACAAGAGTCCGATAGACCCTGG
DH	forward	TTCAAAGCACAATGCCTGGCT
	reverse	GTCTAGATTCTCACAAGAGTCCGATAGACCCTGG
Cμ	forward	TGGCCATGGGCTGCCTAGCCCGGGACTT
	reverse	GCCTGACTGAGCTCACACAAGGAGGA

Microarray data analysis

Total RNA was isolated in two steps using TRIzol (Life Technologies) followed by RNeasy Mini-Kit (Qiagen) purification, following the manufacturer's RNA Clean-up Protocol with the optional On-Column DNase treatment. The integrity and the quality of the RNA were verified by electrophoresis, and its concentration was measured. Samples were analyzed using Affymetrix Mouse Gene 1.0 ST arrays.

Briefly, the robust microarray analysis algorithm was used for background correction, intramicroarray and intermicroarray normalization, and expression signal calculation (21–23). Once the absolute expression signal for each gene (i.e., the signal value for each probeset) was calculated in each microarray, a method called significance analysis of microarray (24) was applied to calculate significant differential expression and find the genes that characterized the impact of ruxolitinib treatment in $Pax5^{+/-}$ $B220^+$ BM cells from mice treated with ruxolitinib for 2 weeks ($n = 4$) compared with untreated $Pax5^{+/-}$ mice ($n = 4$). In the same way, the gene expression of WT BM $B220^+$ cells from mice treated with ruxolitinib for 2 weeks ($n = 5$) was compared with nontreated WT $B220^+$ cells ($n = 5$). The method uses permutations to provide a robust statistical inference of the most significant genes and provides P values adjusted to multiple testing using FDR (25). A cutoff of FDR < 0.015 was used for the differential expression calculations. We applied all methods using R (https://www.r-project.org/; ref. 26) and Bioconductor (27). Gene set enrichment analyses were performed using GSEAv2.2.2 (28, 29) and hallmark collection of gene sets (30).

Whole-genome sequencing

Genomic DNA libraries were prepared from sheared DNA (BM or LN tumor samples with more than 70% blast cells and germline tail DNA samples) with the HyperPrep Library Preparation Kit (Roche PN 07962363001). Paired-end 150 cycle sequencing was performed on a NovaSeq 6000 (Illumina). Illumina paired-end reads were preprocessed and were mapped to the mouse reference genome (mm10) with BWA (31). We used an ensemble approach to call somatic mutations (SNV/indels) with multiple published tools, including Mutect2 (32), SomaticSniper (33), VarScan2 (34), MuSE (35), and Strelka2 (36). The consensus calls by at least two callers were considered as confident mutations. The consensus call sets were further manually reviewed for the read depth, mapping quality, and strand bias to remove additional artifacts. Somatic copy-number alternations were determined by CNVkit (37). For somatic structural variants (SV), four SV callers were implemented in the workflow for SV calling, including Delly (38), Lumpy (39), Manta (40), and Gridss (41). The SV calls passing the default quality filters of each caller were merged using SURVIVOR (42) and genotyped by SVtyper (43). The intersected call sets were manually reviewed for the supporting soft-clipped and discordant read counts at both ends of a putative SV site using IGV. The validation of the germline *Pax5* exon2 deletion is exemplified in Supplementary Fig. S4G.

Data availability

Authors can confirm that all relevant data are included in the article and/or its Supplementary Data files. The gene expression data discussed in this publication have been deposited in NCBI's Gene Expression Omnibus (GEO; ref. 44) and are accessible through GEO Series accession number: GSE179182.

Statistical analyses

Statistical analyses were performed using GraphPad Prism v5.01 (GraphPad Software). Statistical significance was calculated by two-tailed unpaired *t* test. Data normality was tested using the D'Agostino and Pearson test (alpha level = 0.05). Survival analyses were performed using the log-rank/Mantel–Cox test. Two-side Fisher exact test was used to compare leukemia incidence. *P* values are depicted on the figures only for significant differences. According to power analysis calculations, assuming development of leukemia as the experimental endpoint, and an expected proportion of 0.23 B-ALL–positive untreated animals at 20 months of age, a sample size of 34 in each group has a 73% power to detect a decrease in the incidence of the disease to a proportion of 0.03 B-ALL–positive mice in ruxolitininib-treated animals, with a significance level (alpha) of 0.05.

Results

In vivo ruxolitinib delivery in *Pax5*$^{+/-}$ mice

JAK inhibitors are widely used in the clinic to alleviate overactivation of the immune system (45). However, there is potential for immune suppression and subsequent risk for infection. Consequently, proper scheduling of JAK inhibition is essential to achieve maximal anti-preleukemic B-cell activity while minimizing side effects. Toward this end, the JAK2 inhibitor CHZ868 was tolerated at a dose of 30 mg/kg/day in NSG mice for up to 25 days and in immunocompetent mice for up to 44 days, with no obvious effects on PB counts (46). Similarly, lymphocytic choriomeningitis virus-infected *Prf1*$^{-/-}$ mice and lethally irradiated C57BL/6 mice transplanted with cells harboring an activating *Jak2* mutation, have been treated with the JAK1/2 inhibitor ruxolitinib at doses of 90 mg/kg twice daily for up to 1 month and do not show any signs of ruxolitinib-mediated weight loss or other toxicities (47, 48). In humans, ruxolitinib has been used to treat adults with myelofibrosis for up to 5 years or more (49), and adolescents and adults with steroid refractory GVHD for up to 1 year or more (50). In both of these human studies, cytopenias were the most common hematologic adverse events; however, they often normalized or could be managed with ruxolitnib dose reduction. Together, these data suggest that JAK inhibitors such as ruxolitinib are tolerable and provide a therapeutic index for treatment (46, 51).

We first identified the appropriate dose and schedule for ruxolitinib administration in the *in vivo* treatment of *Pax5*$^{+/-}$ mice, where leukemia spontaneously occurs upon natural infection exposure (9). It is possible that ruxolitinib-treated *Pax5*$^{+/-}$ mice kept in a common infectious environment could exhibit an increased frequency of infections due to suppression of immunity as a consequence of JAK1/2 inhibition. To identify an appropriate dose and exposure, we conducted a pilot pharmacokinetic study in which *Pax5*$^{+/-}$ mice were fed with food pellets containing two different concentrations of ruxolitnib for a period of 14 days (**Fig. 1A**). Food pellet dosing is ideal for long-term treatments, especially in distressed disease animal models where repeated oral gavage or other invasive approaches can prove detrimental. Furthermore, ruxolitinib has the appropriate pharmacokinetic (e.g., bioavailability, half-life) and chemical (e.g., stability, formulation) properties (52, 53) to be formulated in food. Dosing via food gives a sustained compound exposure with high levels in the active dark phase of the mice and lower levels in the inactive light phase. Through this approach, we aimed to identify a ruxolinib dose and exposure that was neither myelosuppressive nor immunosuppressive, but pharmacologically active in inhibiting JAK signaling. Ruxolitinib was given at either 0.375 or 0.75 g/kg of food. On the basis of previously observed, average food intake (4 g/day) and body weight (25 g) of *Pax5*$^{+/-}$ mice, these ruxolitinib formulations correspond to doses of approximately 60 and 120 mg/kg/day, respectively. These daily dose levels were previously shown to be well tolerated and pharmacologically active in mouse disease models (48, 51, 54). During the pilot pharmacokinetic study, the average food intake of the *Pax5*$^{+/-}$ mice was 4–5 g/day/mouse (**Fig. 1B**). For the 0.75 g/kg formulation, we anticipated an exposure of 1–3 μmol/L, similar to the C_{max} expected for oral dosing at the corresponding same daily dose (120 mg/kg/day or 60 mg/kg twice daily). Indeed, this exposure was achieved in the active dark phase for several days during the treatment period (**Fig. 1C**). In contrast, with dosing at 0.375 g/kg (corresponding to an oral dose of 60 mg/kg/day or 30 mg/kg twice daily), we observed lower exposures of 0.5 to 0.7 μmol/L C_{max} in the active dark phase for most of the days during the treatment period (**Fig. 1C**). Because the C_{max} in myelofibrosis patients at a maximally tolerated dose of 25 mg twice daily is approximately 1.2 μmol/L (53), the 0.75 g/kg formulation was chosen for all subsequent experiments as it mirrored clinically relevant inhibition of JAK1/2 signaling in humans.

Transient JAK/STAT pathway inhibition selectively targeted susceptible B cells *in vivo*

Pax5$^{+/-}$ mice have an expanded IL7-dependent immature B-cell compartment, from which the leukemic cells are believed to arise (9). Therefore, we next studied whether treatment with ruxolitinib targeted this immature B-cell compartment in *Pax5*$^{+/-}$ mice. To this end, *Pax5*$^{+/-}$ and WT mice received either vehicle or ruxolitinib, and all animals were euthanized either on day 14 or on day 28 (**Fig. 2A**). On day 14, *Pax5*$^{+/-}$ mice treated with ruxolitinib exhibited a significantly reduced proportion of pro-B and pre-B cells in the BM when compared with nontreated age-matched *Pax5*$^{+/-}$ littermates ($P = 0.0003$; **Fig. 2A**; Supplementary Fig. S1A and S1B). This decrease was much more evident after 28 days of ruxolitinib treatment ($P < 0.0001$) and at that later time pro-B and pre-B cells from ruxolitinib-treated WT mice are also affected ($P = 0.0018$; **Fig. 2A**; Supplementary Fig. S1A and S1B). However, 1-year-old *Pax5*$^{+/-}$ mice receiving ruxolitinib for 28 days and not developing B-ALL showed a precursor B-cell population similar to treated 1-year-old WT (**Fig. 2B**; Supplementary Fig. S1C). These findings are consistent with our prior studies in which *in vitro* treatment with ruxolitinib increased cell death of IL7-dependent pro-B cells from WT and *Pax5*$^{+/-}$ mice, with *Pax5*$^{+/-}$ cells most greatly affected (9). Treatment of WT and *Pax5*$^{+/-}$ mice with ruxolitinib for 4 weeks caused a transient increase in the proportions of B cells and granulocytes and a concomitant decrease in the proportions of T cells ($CD4^+$ and $CD8^+$) in the PB (Supplementary Fig. S1D and S1E). Taken together, these results show that transient treatment with ruxolitinib targets immature B cells and exerts rather modest effects on the frequencies of mature immune cells in the blood.

Transient JAK/STAT pathway inhibition targets preleukemic cells via a cell-autonomous mechanism

JAK1/2 inhibitors are widely used in the clinic to alleviate the exacerbated activation of the immune system and prior studies have shown abnormal profiles of inflammatory markers in neonatal blood spot samples of children who later developed B-ALL (55). To explore the mechanism of immature B-cell susceptibility to JAK/STAT pathway inhibition, we next explored whether the decrease of preleukemic B cells in *Pax5*$^{+/-}$ mice after transient ruxolitinib treatment is in part due to dysregulated expression of inflammatory cytokines. To this end, we measured concentrations of inflammatory cytokines (IL2, IL4, IL6, IL10, IL17a, IFNγ, TNFα, and IL1b) in the serum of WT and *Pax5*$^{+/-}$

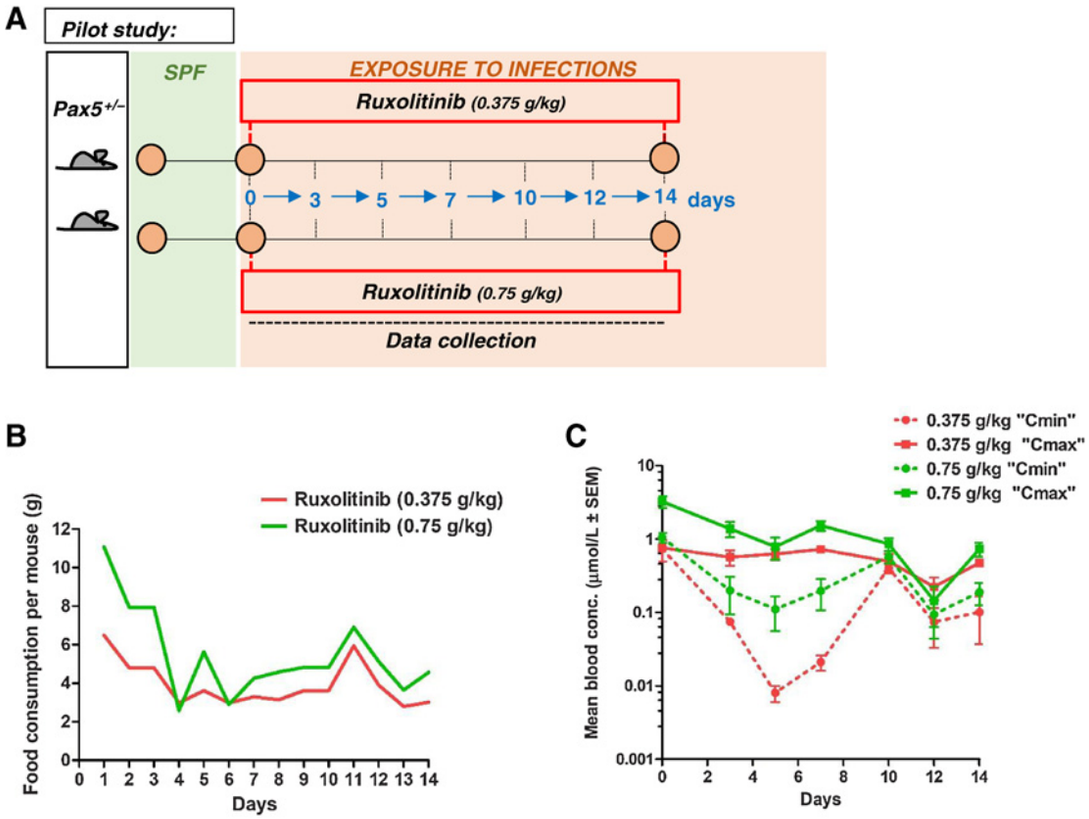

Figure 1.

Ruxolitinib pilot study. **A,** Experimental plan for ruxolitinib pilot study. *Pax5*$^{+/-}$ (gray) mice were born under SPF conditions (green). Two groups of 3-month-old *Pax5*$^{+/-}$ mice were treated for 14 days with two different doses of ruxolitinib ($n = 5$; 0.375 g/kg food and $n = 5$; 0.75 g/kg food) at the time of exposure to infections (orange). Blood samples were collected 2 hours after start of the active dark phase (corresponding to C_{max}) and 2 hours prior to the end of the inactive light phase (corresponding to C_{min}) three times per week during the treatment period. **B,** Food consumption per cage was measured daily and back calculated to an average food intake per mouse per day. **C,** Ruxolitinib concentration in the blood was determined by LC/MS-MS for the different doses of ruxolitinib being examined. Mean blood concentration ± SEM for each day and at the corresponding phase (active: C_{max} or inactive: C_{min}) is represented in the graph.

mice before and after transient ruxolitinib treatment. We found that WT and *Pax5*$^{+/-}$ mice had similar cytokine concentrations in serum samples taken before and after ruxolitinib treatment (Supplementary Fig. S1F). Thus, the decrease of preleukemic B cells is not associated with an obvious change in the serum cytokine profile. This finding suggests that the decrease of preleukemic B cells may be cell autonomous. In agreement with these findings, expression array analysis of preleukemic BM B220^{+} cells derived from *Pax5*$^{+/-}$ mice after ruxolitinib treatment for 2 weeks shows a distinct expression pattern compared with BM B220^{+} cells derived from untreated *Pax5*$^{+/-}$ mice (**Fig. 2C** and **D**; Supplementary Table S1). This change in expression pattern was specific to the *Pax5*$^{+/-}$ genetic background as WT mice treated with ruxolitinib underwent a different pattern of gene expression alterations (**Fig. 2C** and **E**; Supplementary Table S2). We found that, due to the treatment, 1,504 gene-probe sets (FDR = 0.015; **Fig. 2D**; Supplementary Table S1) were differentially expressed in *Pax5*$^{+/-}$ B220^{+} BM cells compared with the same cell population from untreated *Pax5*$^{+/-}$ mice ($n = 4$). Most of the genes ($n = 1,443$) were transcriptionally downregulated with some of these implicated in B-cell development and B-cell receptor signaling (e.g., *Syk*, *Pax5*, *CD79a*, *CD79b*, *Btk*, or *IL6st*; **Fig. 2D**). In contrast, these same genes were not affected in WT mice treated with ruxolitinib ($n = 5$) in which the treatment only affects the gene expression of 294 genes (FDR = 0.015; **Fig. 2E**; Supplementary Table S2). Using the hallmark collection from the Molecular Signatures Database 7.1 (MSigDB; ref. 29), we found that preleukemic BM B220^{+} cells from *Pax5*$^{+/-}$ and WT mice treated with ruxolitinib for 2 weeks were enriched for several hallmark gene sets (Supplementary Fig. S2A and S2B), as well as the apoptosis and p53 pathways (Supplementary Fig. S2C). As expected, genes engaged in IL2 and IL6 signaling were also enriched as a consequence of the cell death induced by ruxolitinib treatment and the association between *Pax5* heterozygosity and production of inflammatory cytokines such as IL6 (Supplementary Fig. S2D; ref. 56). Moreover, genes engaged in the IL7 signaling pathway were selectively downregulated in *Pax5*$^{+/-}$ mice after ruxolitinib treatment (Supplementary Fig. S2E). Taken together, these results reveal that ruxolitinib treatment exerts potent and at times differential effects in *Pax5*$^{+/-}$ versus WT BM B220^{+} cells in terms of global transcriptional program, with potential impacts on B-cell ontogeny, BCR signaling, apoptosis induction, and cytokine signaling.

Transient JAK/STAT pathway inhibition prevents B-ALL development in *Pax5*$^{+/-}$ mice

Building upon these findings, we next examined whether transient ruxolitinib treatment *in vivo* might prevent B-ALL development in *Pax5*$^{+/-}$ mice. We have previously reported that when *Pax5*$^{+/-}$ mice

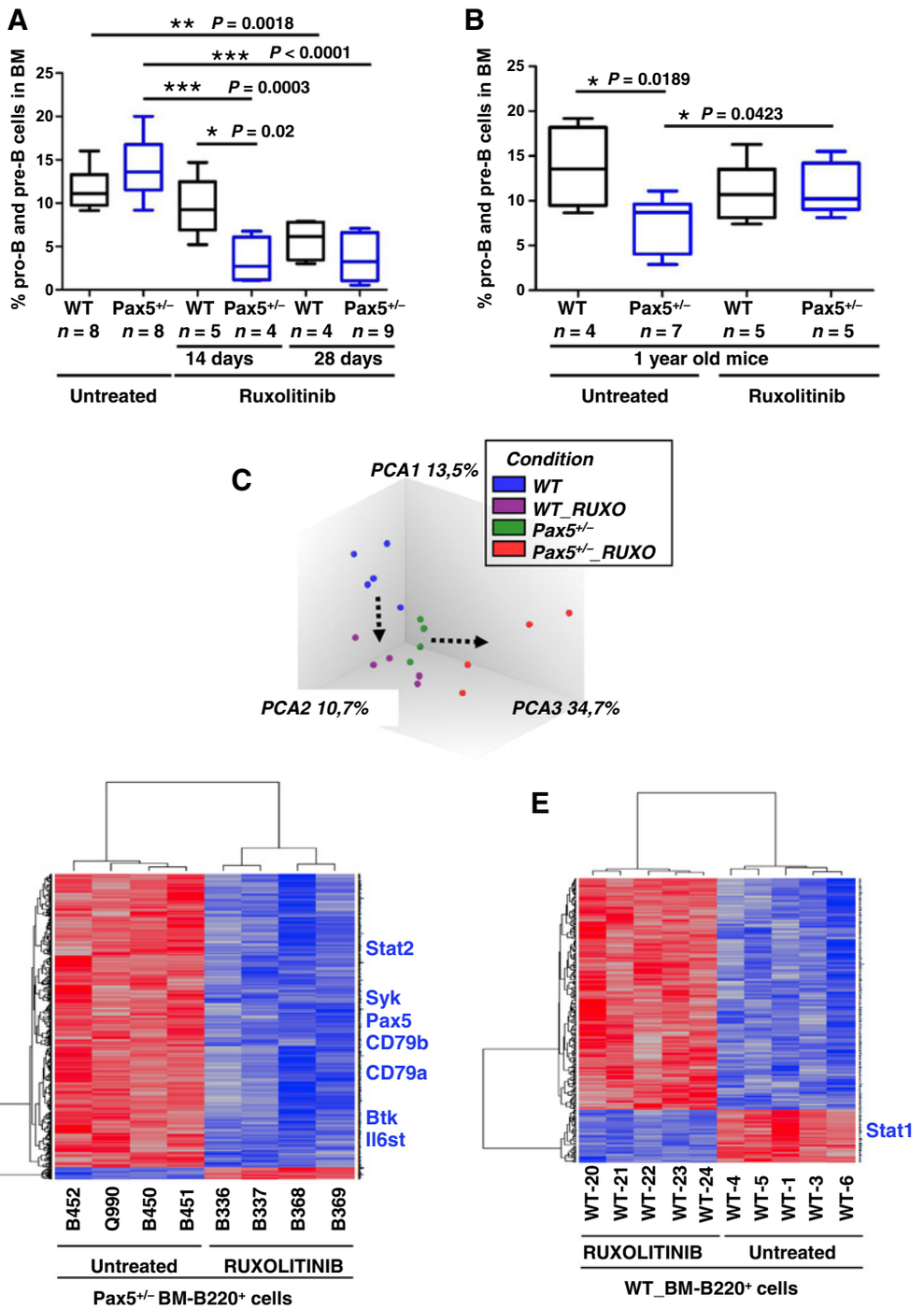

Figure 2.

Impact of ruxolitinib in preleukemic cells. **A,** Flow cytometric analysis of *Pax5*$^{+/-}$ ($n = 4$–9) and WT ($n = 4$–8) mice treated with ruxolitinib (for 14 or 28 days) identified a significant decrease of bone marrow pro-B and pre-B cells (B220^{low}IgM^{-}) due to the treatment. Box plots horizontal bars represent the mean ± SD. To determine statistical significance, an unpaired *t* test was used. **B,** Percentage of BM pro-B and pre-B cells (B220^{low}IgM^{-}) of 1-year-old *Pax5*$^{+/-}$ ($n = 5$) and WT ($n = 5$) mice that were previously treated with ruxolitinib for 28 days and compared with age-matched untreated *Pax5*$^{+/-}$ ($n = 7$) and WT ($n = 4$) mice. Box plots horizontal bars represent the mean ± SD. To determine statistical significance, an unpaired *t* test was used. **C,** Principal component analysis plot showing the differences in gene expression of B220^{+} BM cells from *Pax5*$^{+/-}$ mice treated with ruxolitinib (red dots; $n = 4$), untreated *Pax5*$^{+/-}$ mice (green dots; $n = 4$), ruxolitinib-treated WT mice (purple dots; $n = 5$), and untreated WT mice (blue dots; $n = 5$). Dotted arrows represent the ruxolitinib treatment effect on gene expression of B220^{+} BM cells from WT and *Pax5*$^{+/-}$ mice. RUXO, ruxolitinib. **D,** Unsupervised heatmap showing the significant differentially expressed genes (1,504 genes-probesets) between B220^{+} bone marrow cells from *Pax5*$^{+/-}$ mice treated with ruxolitinib during 2 weeks ($n = 4$) and *Pax5*$^{+/-}$ untreated mice ($n = 4$). **E,** Unsupervised heatmap showing the significant differentially expressed genes (294 genes-probesets) between B220^{+} BM cells from control-WT mice treated with ruxolitinib during 2 weeks ($n = 5$) and control-WT untreated mice ($n = 5$). The significance analysis of microarrays was defined by an FDR = 0.015%.

were moved to a conventional facility in the presence of infectious agents, 22% of the animals developed B-ALL and the leukemia occurred between 6 and 16 months of age (9). Therefore, we established a mouse cohort consisting of 42 control littermate WT and 71 *Pax5*$^{+/-}$ mice. All mice were born in a SPF facility. Four weeks after birth, mice were transferred to a conventional facility, and 19 WT and 29 *Pax5*$^{+/-}$ mice were fed with pellets containing ruxolitinib for 4 weeks, 8 *Pax5*$^{+/-}$ mice were fed with pellets ruxolitinib for 2 weeks, and the remaining 23 WT and 34 *Pax5*$^{+/-}$ mice received pellets containing vehicle (**Fig. 3A**). The microbiologic status of mice was monitored before and periodically throughout treatment, with no differences observed between treated and untreated animals (Supplementary Table S3). Consistent with our previous findings, 8 of 34 (23.52%) *Pax5*$^{+/-}$ mice receiving vehicle developed and succumbed to leukemia (**Fig 3B** and **C**). In contrast, the B-ALL incidence was significantly decreased after treatment with ruxolitinib, where only 1 of 29 (3.4%) *Pax5*$^{+/-}$ mice developed and died from disease ($P = 0.0332$; **Fig 3B** and **C**). Curiously, when *Pax5*$^{+/-}$ mice were treated with ruxolitinib for 14 instead of 28 days, the incidence of B-ALL (2/8, 25%) was similar to *Pax5*$^{+/-}$ mice that had not been treated with the inhibitor (**Fig 3C**). Thus, ruxolitinib treatment reduces B-ALL risk, with leukemia prevention occurring in a time-dependent manner, presumably to ensure eradication of maximal numbers of susceptible immature B cells.

B-ALL onset in vehicle and ruxolitinib treated mice occurred between 7 and 15 months of age (**Fig. 3B**) and became manifest by the appearance of blast cells in the PB, BM, spleen, and LNs (**Fig. 3D** and E; Supplementary Fig. S3A–S3C). Flow cytometric analysis revealed the expected CD19^{+}B220^{low}IgM^{-}CD25^{+} cell surface phenotype for leukemic blasts, regardless of their location (**Fig. 3D**; Supplementary Fig. S3B and S3C). None of the ruxolitinib-treated WT mice developed hematologic or other malignancies over the time course of this experiment (**Fig. 3B**; Supplementary Fig. S3D). The leukemic *Pax5*$^{+/-}$ mouse treated with ruxolitinib also displayed clonal immunoglobulin VH-DJH and D-JH gene rearrangements consistent with a pro-B or pre-B cell of origin (Supplementary Fig. S3E).

To identify somatically acquired second hits leading to B-ALL development in ruxolitinib-treated or untreated *Pax5*$^{+/-}$ mice, we performed whole-genome sequencing of paired tumor and germline tail DNA samples from 8 leukemic *Pax5*$^{+/-}$ mice, including 7 vehicle and 1 ruxolitinib-treated animal. The percentage of leukemic cells for each mouse was: 95% (A428) from total BM, 94% (A707) from total BM, 70% (A733) from total BM, 91% (L832) from total BM, 95% (L380) from total BM, 80% (A734) from total LN, 85% (L712) from total BM and 90% (W471) from total LN. We identified several somatically acquired recurrent mutations and copy-number variations involving B-cell transcription factors in diseased *Pax5*$^{+/-}$ mice of the vehicle-treated cohort (e.g., *Ikzf1*, *Ebf1*; **Fig. 4**; Supplementary Fig. S4A–S4G), similar to those commonly identified in human B-ALL samples. Furthermore, recurrent mutations affecting the JAK/STAT and RAS signaling pathways were detected (**Fig. 4**; Supplementary Fig. S4A–S4G). The leukemia sample from the ruxolitinib-treated mouse harbored similar recurrent mutations in JAK/STAT pathway genes as those identified in leukemic *Pax5*$^{+/-}$ mice from the vehicle treated cohort (**Fig. 4**), suggesting that treatment was not able to eradicate all of the susceptible preleukemic cells in this particular case.

B-cell–restricted *Jak3*^{V670a} expression causes B-ALL in *Pax5*$^{+/-}$ mice with a very short latency

The reduction in B-ALL incidence in ruxolitinib-treated *Pax5*$^{+/-}$ mice could be due to the elimination of preleukemic B cells that already harbor or acquire a leukemogenic JAK/STAT pathway mutation during the 4-week treatment period. This second possibility seems unlikely because previous deep sequencing studies with a depth of 600,000 to 2.5×10^6 reads have shown that somatic *Jak* mutations appear in the blood of *Pax5*$^{+/-}$ mice only at the time that animals manifest with B-ALL (9). However, in our current study, B-ALL does not develop until several months after discontinuing ruxolitinib treatment. Alternatively, it is possible that the lower B-ALL incidence could result from ruxolitinib-mediated elimination or reduction in the number of immature *Pax5*$^{+/-}$ B cells that are susceptible to acquiring activating *Jak* or other leukemogenic mutations. To further address this question, we chose to model leukemia in *Pax5*$^{+/-}$ mice that expressed an activating *Jak3*^{V670A} mutation in the precursor B-cell population. Toward this end, we generated a conditional *Rosa26-mJak3*^{V670A} *Pax5*$^{+/-}$ mouse model and crossed it with an *Mb1-Cre* mouse strain (20). Resulting Cre^{+} animals delete a stop cassette upstream of the mutant *Jak3* allele upon B-lineage commitment at the pro-B-cell stage, leading to expression of the activated *Jak3*^{V670A}. Notably, all *Rosa26-mJak3*^{V670A}+*Mb1-Cre*+*Pax5*$^{+/-}$ mice developed B-ALL with an average latency of 4 weeks after birth and in the absence of infection exposure (**Fig. 5A**). Leukemic mice displayed enlarged LNs at the time of sacrifice (**Fig. 5B**) due to the accumulation of leukemic B cells with a B220^{+}IgM$^{+/-}$CD25^{+}CD19^{+} phenotype that extended throughout the BM, PB, spleen LN (**Fig. 5C**). All *Rosa26-mJak3*^{V670A}+*Mb1-Cre*+*Pax5*$^{+/-}$ B-ALLs displayed clonal immature BCR rearrangements (**Fig. 5D**) and infiltrated non-lymphoid tissues, such as the liver and kidney (**Fig. 5E**). As a control, we developed and characterized *Rosa26-mJak3*^{V670A}+ *Mb1-Cre*+*Pax5*$^{+/+}$ mice. These *Rosa26-mJak3*^{V670A}+*Mb1-Cre*+*Pax5*$^{+/+}$ mice developed leukemia with a larger latency than *Rosa26-mJak3*^{V670A}+*Mb1-Cre*+*Pax5*$^{+/-}$ mice (Supplementary Fig. S5A), but in 100% of the cases, the leukemias were T-ALL (Supplementary Fig. S5B and S5C). These findings support the notion that Pax5 downregulation is required to establish a malignant B-cell identity during ALL development (6, 57, 58). Overall, these data are not consistent with a model in which *Jak* mutations are present in one or a few cells from birth and suggest that ruxolitinib treatment reduces leukemia risk by decreasing the number of early susceptible B cells in which these mutations later arise.

Discussion

Numerous preclinical studies have demonstrated that a gene–environment interaction is linked to the development of childhood B-ALL in the context of germline pathogenic *Pax5* variants and the somatic *ETV6-RUNX1* translocation (9, 11). These studies reveal that infectious exposure increase the likelihood of B-ALL development as the result of an increased sensitivity of B-cell precursors harboring specific genetic variants to transformation. Collectively, these findings encourage the study of novel interventions to prevent childhood leukemia development (6, 59). Although the exact nature of this gene–environment interaction remains unknown (reviewed in refs. 6, 57, 58), the characterization of preleukmic B cells might identify vulnerabilities to inform development of prevention strategies. Such is the case for *Pax5*$^{+/-}$ preleukemic B cells, where we previously demonstrated that *Pax5* heterozygosity creates an aberrant IL7-sensitive precursor B-cell compartment that is exquisitely sensitive to ruxolitinib *in vitro* (9). In the current study, we demonstrate for the first time that eliminating this susceptible precursor population by ruxolitinib treatment *in vivo* prevents the development of B-ALL.

Through this investigation, we demonstrate that the incidence of B-ALL is reduced in *Pax5*$^{+/-}$ mice in an infectious environment

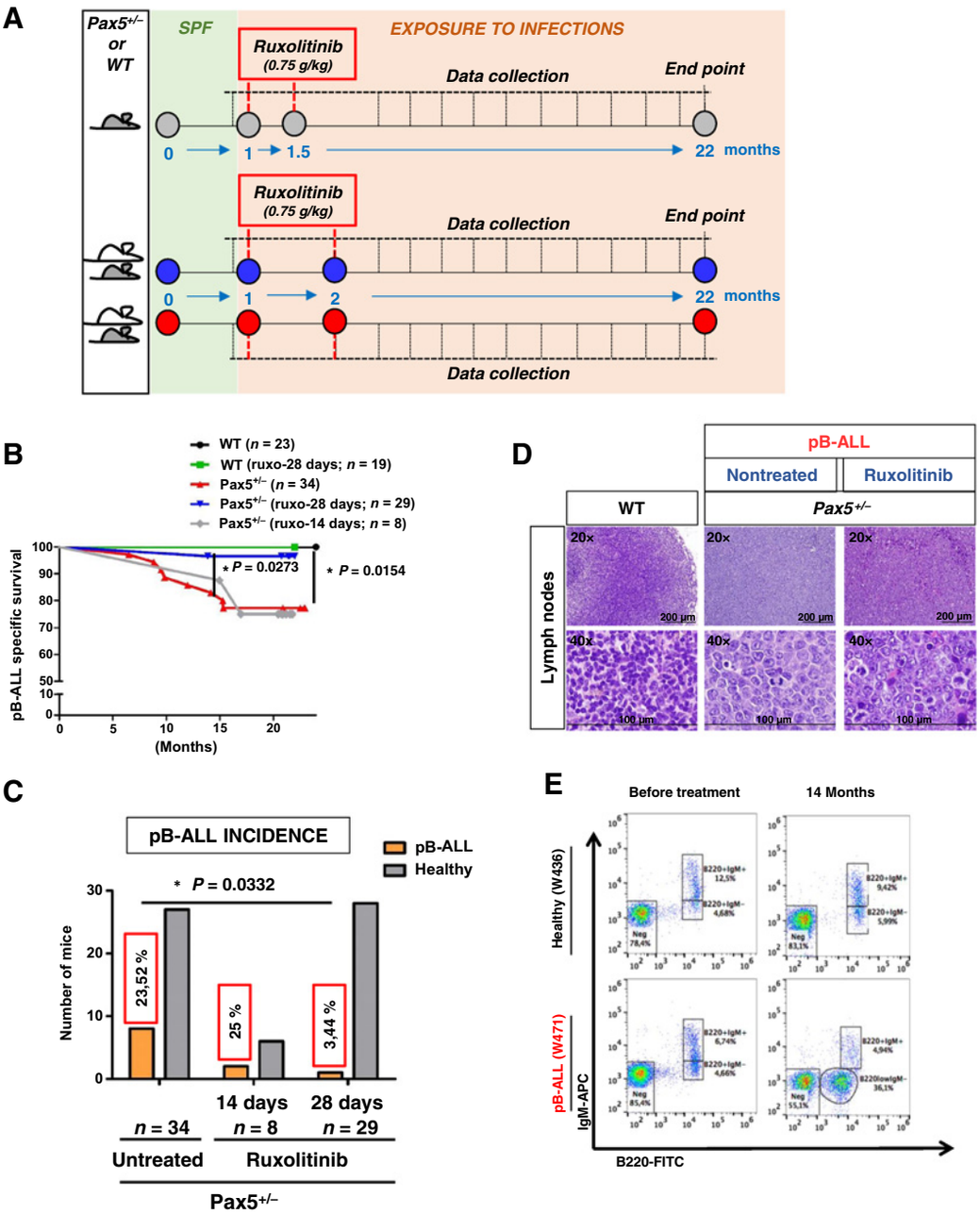

Figure 3.

Ruxolitinib treatment prevents infection-driven B-ALL development in *Pax5*$^{+/-}$ predisposed mice. **A,** Study design. *Pax5*$^{+/-}$ (gray; $n = 71$) and *WT* (white; $n = 42$) mice were born under SPF conditions (green). After 1 month of age, the mice were transferred to a conventional facility providing a natural infectious environment (orange). At the time of exposure to infections, a group of *Pax5*$^{+/-}$ mice ($n = 8$) was treated with ruxolitinib (0.75 g/kg food) for 14 days (gray circles). Two additional groups of *Pax5*$^{+/-}$ ($n = 29$) and *WT* ($n = 19$) mice were treated with ruxolitinib (0.75 g/kg food) for 28 days (blue circles) and the remaining *Pax5*$^{+/-}$ ($n = 34$) and *WT* ($n = 23$) mice were treated with vehicle (red circles). The lifespan of the mice included in the study is indicated by a horizontal blue bar (in months). **B,** B-ALL–specific survival of mice treated with ruxolitinib for 28 days (*Pax5*$^{+/-}$, blue line, $n = 29$; *WT*, green line, $n = 19$), *Pax5*$^{+/-}$ mice treated with ruxolitinib for 14 days (gray line, $n = 8$), and nontreated mice (*Pax5*$^{+/-}$, red line, $n = 34$; *WT*, black line, $n = 23$) following exposure to common infections. Log-rank (Mantel–Cox) test $P = 0.0273$ when comparing *Pax5*$^{+/-}$ mice treated with ruxolitinib for 28 days versus nontreated *Pax5*$^{+/-}$ mice and $P = 0.0154$ when comparing *Pax5*$^{+/-}$ versus *WT* mice without treatment. ruxo, ruxolitinib. **C,** Reduction in pB-ALL incidence in *Pax5*$^{+/-}$ mice treated with ruxolitinib for 4 weeks. Ruxolitinib treatment of *Pax5*$^{+/-}$ mice for 4 weeks resulted in pB-ALL development in 3.44% of mice compared with a 23.52% of incidence in untreated animals. Fisher exact test, $P = 0.0332$. **D,** Hematoxylin and eosin staining of tumor-bearing *Pax5*$^{+/-}$ mice showing infiltrating blast cells in the LN, compared with an age-matched WT mouse. Loss of normal architecture due to leukemic cell infiltration can be seen. Magnification and the corresponding scale bar are indicated in each case. **E,** Flow cytometric analysis of PB showing the accumulation of blast B cells (B220^{low} IgM^{-}) in the leukemic *Pax5*$^{+/-}$ mouse (W471) and compared with a healthy *Pax5*$^{+/-}$ mouse (W436), both treated with ruxolitinib (120 mg/kg/day) and exposed to common infections.

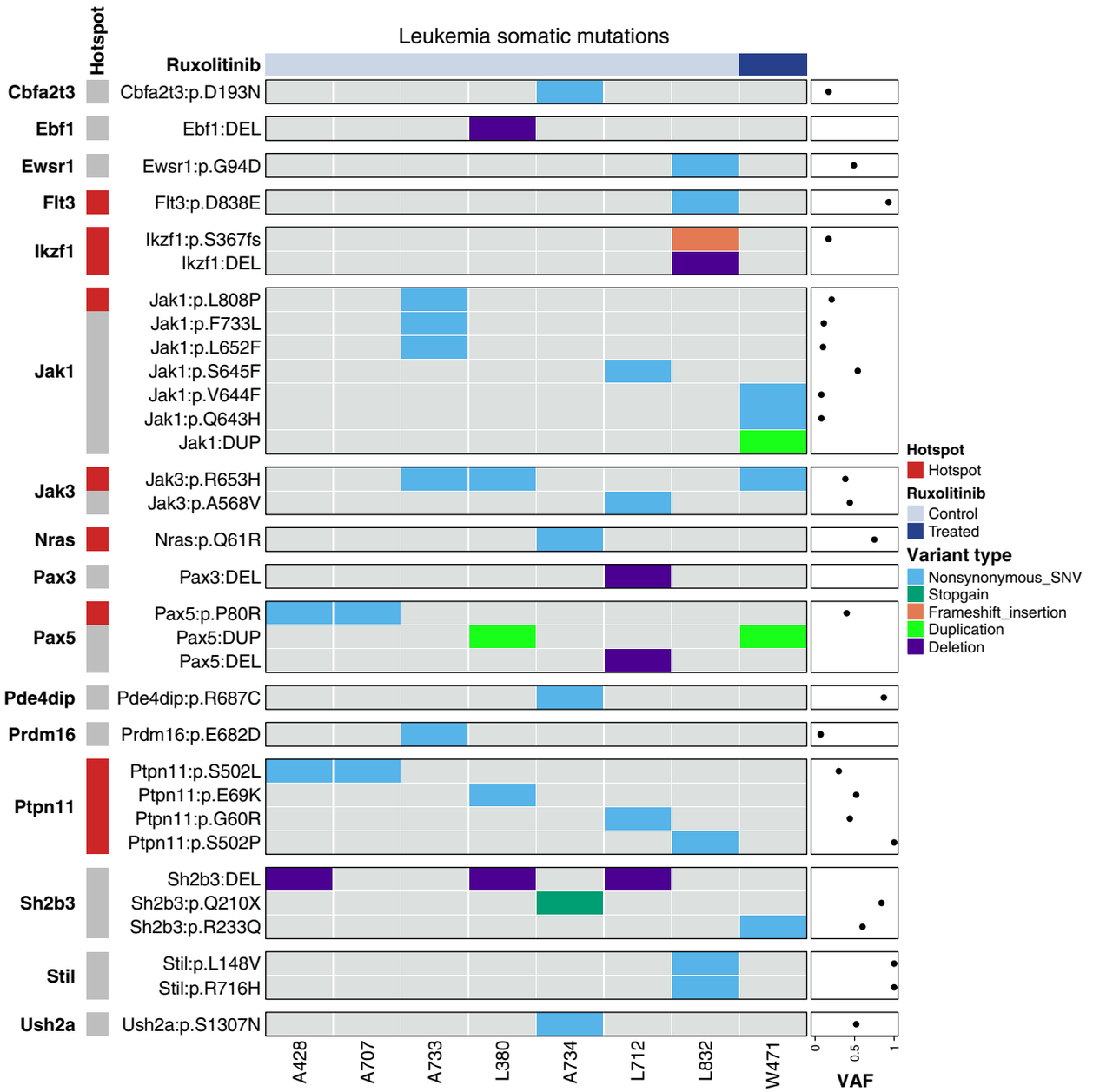

Figure 4.

Whole-genome sequencing in leukemic *Pax5*$^{+/-}$ mice. Oncoprint of somatic single-nucleotide mutations and copy-number alterations across seven leukemia samples from *Pax5*$^{+/-}$ control mice (light blue) and one leukemia from *Pax5*$^{+/-}$ ruxolitinib-treated mouse (dark blue). Somatic alterations are clustered by gene. Tumor DNA was derived from whole leukemic BM or LN, while tail DNA of the respective mouse was used as reference germline material. Previously reported known human or mouse leukemia hotspot mutations are highlighted (red). Mean tumor variant allele fraction for each single nucleotide mutation is shown on the dot plot on the right.

following transient and early administration of the JAK inhibitor ruxolitinib. These findings support the hypothesis that children who are genetically predisposed to B-ALL might similarly benefit from early transient JAK/STAT pathway inhibition as a preventive strategy. Because we also see a reduction in the immature B-cell population in WT mice, it is possible that such an approach might prove useful for other forms of ALL prevention—such as in children whose bone marrow cells harbor the t(12; 21) translocation. The clinical approach will require delivering the intervention at the most appropriate temporal window and in a child-tailored manner (59). One option might be to monitor the blood of predisposed children for the emergence of leukemogenic clone with second hit mutations, such as those affecting the *JAK*s, and when detected, initiate treatment. However, waiting for the emergence of such clones might be too late in the disease course. Furthermore, ruxolitinib treatment would not be expected to cure leukemia because it does not target Jak3, which is

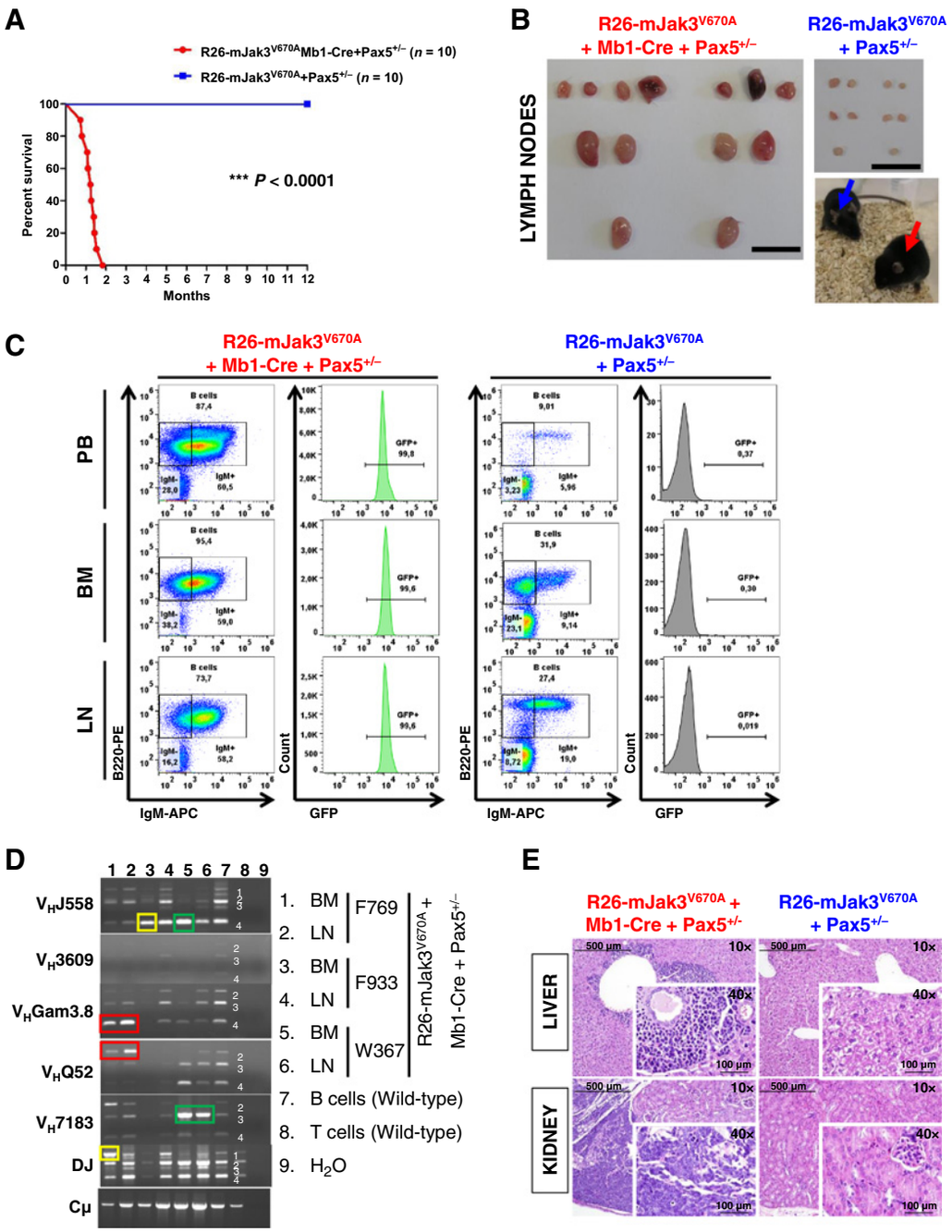

Figure 5.

B-ALL development in *Rosa26-mJak3*^{V670A}+*Mb1-Cre*+ *Pax5*$^{+/-}$ mice. **A,** Overall survival of *Rosa26-mJak3*^{V670A}+*Mb1-Cre*+*Pax5*$^{+/-}$ (red line; $n = 10$) and *Rosa26-mJak3*^{V670A}+*Pax5*$^{+/-}$ mice (blue line; $n = 10$), none of them exposed to common infections. Log-rank (Mantel–Cox) test, $P < 0.0001$. **B,** Photographs of the LNs of 1,7 month-old sibling *Rosa26-mJak3*^{V670A}+*Mb1-Cre*+*Pax5*$^{+/-}$ (red arrow) and *Rosa26-mJak3*^{V670A}+*Pax5*$^{+/-}$ mice (blue arrow). Scale bars, 1 cm. **C,** Flow cytometric analysis of B-cell subsets in diseased *Rosa26-mJak3*^{V670A}+*Mb1-Cre*+*Pax5*$^{+/-}$ mice. Representative plots of B cell from the PB, BM, and LNs are shown. B cells from a control littermate *Rosa26-mJak3*^{V670A}+*Pax5*$^{+/-}$ mouse are shown for reference. Tracking of the GFP marker for *mJak3*^{V670A} transgene expression in the leukemic B cells of *Rosa26-mJak3*^{V670A}+*Mb1-Cre*+*Pax5*$^{+/-}$ mice shows that all tumor cells are GFP^{+} in 100% (10/10) of the mice studied. Flow cytometric images are representative of 10 mice analyzed. **D,** BCR clonality in *Rosa26-mJak3*^{V670A}+*Mb1-Cre*+*Pax5*$^{+/-}$ mice. PCR analysis of BCR gene rearrangements in infiltrated BM and LNs of diseased mice. Sorted CD19^{+} B cells from spleens of healthy mice served as a control for polyclonal BCR rearrangements. DP T cells from the thymus of healthy mice served as a negative control. Leukemic mice show increased clonality within their BCR repertoire (indicated by colored squares). **E,** An example of hematoxylin and eosin staining of liver and kidney from a tumor-bearing *Rosa26-mJak3*^{V670A}+*Mb1-Cre*+*Pax5*$^{+/-}$ mouse shows infiltrates of relatively uniform lymphoid cells with immature appearance. The same tissues from a control littermate *Rosa26-mJak3*^{V670A}+*Pax5*$^{+/-}$ mouse are shown as reference.

commonly mutated in *Pax5*$^{+/-}$ leukemic blasts. Consistent with these possibilities, treatment with ruxolitinib fails to completely eradicate leukemic blasts in mice infused with *Pax5*$^{+/-}$ pro-B cells harboring an activating *Jak3* mutation (9). Alternatively, treatment could be given to predisposed children intermittently during early childhood to target the aberrant B-cell population. In any case, such a preventive approach could apply to other cases where second hits within the leukemic blasts guide the identification of vulnerabilities within the preleukemic B-cell population. Overall, these findings support further investigation of pathway-specific approaches to target preleukemic B cells as a means to prevent B-ALL onset in the future.

Authors' Disclosures

O. Blanco reports personal fees from Takeda and Clinigen outside the submitted work. T. Radimerski reports personal fees from Novartis Pharma AG outside the submitted work and is a holder of Novartis stock. J.J. Yang reports grants from Takeda Pharmaceutical Company outside the submitted work. A. Weiss is an employee and shareholder of Novartis Pharma AG. K.E. Nichols reports grants from Incyte outside the submitted work. No disclosures were reported by the other authors.

Authors' Contributions

A. Casado-García: Validation, investigation, methodology, writing–original draft. **M. Isidro-Hernández:** Validation, investigation, methodology, writing–original draft. **N. Oak:** Validation, investigation, methodology, writing–original draft. **A. Mayado:** Validation, investigation, methodology, writing–review and editing. **C. Mann-Ran:** Validation, investigation, methodology, writing–review and editing. **J. Raboso-Gallego:** Validation, investigation, methodology, writing–review and editing. **S. Alemán-Arteaga:** Validation, investigation, methodology, writing–review and editing. **A. Buhles:** Validation, investigation, methodology, writing–review and editing. **D. Sterker:** Validation, investigation, methodology, writing–review and editing. **E.G. Sánchez:** Validation, investigation, methodology, writing–review and editing. **J. Martínez-Cano:** Validation, investigation, methodology, writing–review and editing. **O. Blanco:** Validation, investigation, methodology, writing–review and editing. **A. Orfao:** Resources, supervision, investigation, writing–review and editing. **D. Alonso-López:** Software, formal analysis, investigation, methodology, writing–review and editing. **J. De Las Rivas:** Formal analysis, supervision, writing–review and editing. **S. Riesco:** Formal analysis, investigation, methodology, writing–review and editing. **P. Prieto-Matos:** Formal analysis, investigation, methodology, writing–review and editing. **A. González-Murillo:** Formal analysis, investigation, methodology, writing–review and editing. **F.J. Garcia Criado:** Formal analysis, investigation, methodology, writing–review and editing. **M.B. Garcia Cenador:** Formal analysis, investigation, methodology, writing–review and editing. **T. Radimerski:** Conceptualization, resources, formal analysis, supervision, funding acquisition, methodology, writing–original draft. **M. Ramírez-Orellana:** Conceptualization, resources, formal analysis, supervision, funding acquisition, investigation, writing–original draft. **C. Cobaleda:** Resources, formal analysis, supervision, investigation, writing–original draft. **J.J. Yang:** Resources, supervision, funding acquisition, investigation, writing–review and editing. **C. Vicente-Dueñas:** Conceptualization, resources, formal analysis, supervision, funding acquisition, validation, investigation, methodology, writing–original draft. **A. Weiss:** Conceptualization, resources, formal analysis, supervision, funding acquisition, investigation, methodology, writing–original draft. **K.E. Nichols:** Conceptualization, resources, formal analysis, supervision, funding acquisition, investigation, methodology, writing–original draft. **I. Sánchez-García:** Conceptualization, resources, formal analysis, supervision, funding acquisition, investigation, methodology, writing–original draft.

Acknowledgments

The authors thank all the members of their laboratories for discussion. Research at C. Cobaleda's laboratory was partially supported by FEDER MINECO (SAF2017-83061-R), the "Fundación Ramón Areces" and a Research Contract with the "Fundación Síndrome de Wolf-Hirschhorn o 4p-". Institutional grants from the "Fundación Ramón Areces" and "Banco de Santander" to the CBMSO are also acknowledged. The authors also thank the Hartwell Center and Dr. Ti-Cheng Chang from the Center for Bioinformatics at SJCRH for their support in whole-genome sequence and bioinformatic pipelines.

C. Cobaleda and C. Vicente-Dueñas labs are members of the EU COST Action LEGEND (CA16223). Research in C. Vicente-Dueñas group has been funded by Instituto de Salud Carlos III through the project " PI17/00167 and by a "Miguel Servet Grant" [CPII19/00024 - AES 2017-2020; co-funded by European Regional Development Fund (ERDF)/European Social Fund (ESF) "A way to make Europe"/ "Investing in your future"]. J.J. Yang and K.E. Nichols receive funding from the American Lebanese Syrian Associated Charities (ALSAC) and R01CA241452 from the NCI. Research in ISG group is partially supported by FEDER and by SAF2015-64420-R MINECO/FEDER, UE, RTI2018-093314-B-I00 MCIU/AEI/FEDER, UE, 9659122185-122185-4-21 MCIU/AEI/FEDER, UE, by Junta de Castilla y León (UIC-017, CSI001U16, CSI234P18, and CSI144P20). M. Ramírez-Orellana and I. Sánchez-García have been supported by the Fundacion Unoentrecienmil (CUNINA project). C. Cobaleda, M. Ramírez-Orellana, and I. Sánchez-García have been supported by the Fundación Científica de la Asociación Española contra el Cáncer (PRYCO211305-SANC). A. Casado-García (CSI067-18) and M. Isidro-Hernández (CSI021-19) are supported by FSE-Conserjería de Educación de la Junta de Castilla y León 2019 and 2020 (ESF, European Social Fund) fellowship, respectively. J. Raboso-Gallego is supported by a scholarship from University of Salamanca co-financed by Banco Santander and ESF. S. Alemán-Arteaga is supported by an Ayuda para Contratos predoctorales para la formación de doctores (PRE2019-088887).

The costs of publication of this article were defrayed in part by the payment of page charges. This article must therefore be hereby marked *advertisement* in accordance with 18 U.S.C. Section 1734 solely to indicate this fact.

Received October 6, 2021; revised December 14, 2021; accepted January 24, 2022; published first February 7, 2022.

References

1. Hunger SP, Mullighan CG. Acute lymphoblastic leukemia in children. N Engl J Med 2015;373:1541–52.
2. Linabery AM, Ross JA. Trends in childhood cancer incidence in the U.S. (1992–2004). Cancer 2008;112:416–32.
3. Smith MA, Seibel NL, Altekruse SF, Ries LA, Melbert DL, O'Leary M, et al. Outcomes for children and adolescents with cancer: challenges for the twenty-first century. J Clin Oncol 2010;28:2625–34.
4. Schafer D, Olsen M, Lahnemann D, Stanulla M, Slany R, Schmiegelow K, et al. Five percent of healthy newborns have an ETV6-RUNX1 fusion as revealed by DNA-based GIPFEL screening. Blood 2018;131:821–6.
5. Vicente-Duenas C, Janssen S, Oldenburg M, Auer F, Gonzalez-Herrero I, Casado-Garcia A, et al. An intact gut microbiome protects genetically predisposed mice against leukemia. Blood 2020;136:2003–17.
6. Cobaleda C, Vicente-Duenas C, Sanchez-Garcia I. Infectious triggers and novel therapeutic opportunities in childhood B cell leukaemia. Nat Rev Immunol 2021;21:570–81.
7. Greaves M, Cazzaniga V, Ford A. Can we prevent childhood leukaemia? Leukemia 2021;35:1258–64.
8. Swaminathan S, Klemm L, Park E, Papaemmanuil E, Ford A, Kweon SM, et al. Mechanisms of clonal evolution in childhood acute lymphoblastic leukemia. Nat Immunol 2015;16:766–74.
9. Martin-Lorenzo A, Hauer J, Vicente-Duenas C, Auer F, Gonzalez-Herrero I, Garcia-Ramirez I, et al. Infection exposure is a causal factor in B-cell precursor acute lymphoblastic leukemia as a result of Pax5-inherited susceptibility. Cancer Discov 2015;5:1328–43.
10. Fidanza M, Seif AE, DeMicco A, Rolf N, Jo S, Yin B, et al. Inhibition of precursor B-cell malignancy progression by toll-like receptor ligand-induced immune responses. Leukemia 2016;30:2116–9.
11. Rodriguez-Hernandez G, Hauer J, Martin-Lorenzo A, Schafer D, Bartenhagen C, Garcia-Ramirez I, et al. Infection exposure promotes ETV6-RUNX1 precursor B-cell leukemia via impaired H3K4 demethylases. Cancer Res 2017;77:4365–77.
12. Greaves M. A causal mechanism for childhood acute lymphoblastic leukaemia. Nat Rev Cancer 2018;18:471–84.
13. Rodriguez-Hernandez G, Opitz FV, Delgado P, Walter C, Alvarez-Prado AF, Gonzalez-Herrero I, et al. Infectious stimuli promote malignant B-cell acute lymphoblastic leukemia in the absence of AID. Nat Commun 2019;10:5563.

14. Duployez N, Jamrog LA, Fregona V, Hamelle C, Fenwarth L, Lejeune S, et al. Germline PAX5 mutation predisposes to familial B-cell precursor acute lymphoblastic leukemia. Blood 2021;137:1424–8.
15. Auer F, Ruschendorf F, Gombert M, Husemann P, Ginzel S, Izraeli S, et al. Inherited susceptibility to pre B-ALL caused by germline transmission of PAX5 c.547G>A. Leukemia 2014;28:1136–8.
16. Shah S, Schrader KA, Waanders E, Timms AE, Vijai J, Miething C, et al. A recurrent germline PAX5 mutation confers susceptibility to pre-B cell acute lymphoblastic leukemia. Nat Genet 2013;45:1226–31.
17. Heltemes-Harris LM, Willette MJ, Ramsey LB, Qiu YH, Neeley ES, Zhang N, et al. Ebf1 or Pax5 haploinsufficiency synergizes with STAT5 activation to initiate acute lymphoblastic leukemia. J Exp Med 2011;208:1135–49.
18. Urbanek P, Wang ZQ, Fetka I, Wagner EF, Busslinger M. Complete block of early B cell differentiation and altered patterning of the posterior midbrain in mice lacking Pax5/BSAP. Cell 1994;79:901–12.
19. Mao X, Fujiwara Y, Orkin SH. Improved reporter strain for monitoring Cre recombinase-mediated DNA excisions in mice. Proc Natl Acad Sci U S A 1999; 96:5037–42.
20. Hobeika E, Thiemann S, Storch B, Jumaa H, Nielsen PJ, Pelanda R, et al. Testing gene function early in the B cell lineage in mb1-cre mice. Proc Natl Acad Sci U S A 2006;103:13789–94.
21. Bolstad BM, Irizarry RA, Astrand M, Speed TP. A comparison of normalization methods for high density oligonucleotide array data based on variance and bias. Bioinformatics 2003;19:185–93.
22. Irizarry RA, Bolstad BM, Collin F, Cope LM, Hobbs B, Speed TP. Summaries of Affymetrix GeneChip probe level data. Nucleic Acids Res 2003;31:e15.
23. Irizarry RA, Hobbs B, Collin F, Beazer-Barclay YD, Antonellis KJ, Scherf U, et al. Exploration, normalization, and summaries of high density oligonucleotide array probe level data. Biostatistics 2003;4:249–64.
24. Tusher VG, Tibshirani R, Chu G. Significance analysis of microarrays applied to the ionizing radiation response. Proc Natl Acad Sci U S A 2001;98:5116–21.
25. Benjamini Y, Drai D, Elmer G, Kafkafi N, Golani I. Controlling the false discovery rate in behavior genetics research. Behav Brain Res 2001;125:279–84.
26. Team RDC. A language and environment for statistical computing. R Foundation for Statistical Computing, Vienna, Austria ISBN 3–900051–07–0; 2010.
27. Gentleman RC, Carey VJ, Bates DM, Bolstad B, Dettling M, Dudoit S, et al. Bioconductor: open software development for computational biology and bioinformatics. Genome Biol 2004;5:R80.
28. Mootha VK, Lindgren CM, Eriksson KF, Subramanian A, Sihag S, Lehar J, et al. PGC-1alpha-responsive genes involved in oxidative phosphorylation are coordinately downregulated in human diabetes. Nat Genet 2003;34:267–73.
29. Subramanian A, Tamayo P, Mootha VK, Mukherjee S, Ebert BL, Gillette MA, et al. Gene set enrichment analysis: a knowledge-based approach for interpreting genome-wide expression profiles. Proc Natl Acad Sci U S A 2005;102:15545–50.
30. Liberzon A, Birger C, Thorvaldsdottir H, Ghandi M, Mesirov JP, Tamayo P. The Molecular Signatures Database (MSigDB) hallmark gene set collection. Cell Syst 2015;1:417–25.
31. Li H, Durbin R. Fast and accurate long-read alignment with Burrows-Wheeler transform. Bioinformatics 2010;26:589–95.
32. Cibulskis K, Lawrence MS, Carter SL, Sivachenko A, Jaffe D, Sougnez C, et al. Sensitive detection of somatic point mutations in impure and heterogeneous cancer samples. Nat Biotechnol 2013;31:213–9.
33. Larson DE, Harris CC, Chen K, Koboldt DC, Abbott TE, Dooling DJ, et al. SomaticSniper: identification of somatic point mutations in whole genome sequencing data. Bioinformatics 2012;28:311–7.
34. Koboldt DC, Zhang Q, Larson DE, Shen D, McLellan MD, Lin L, et al. VarScan 2: somatic mutation and copy number alteration discovery in cancer by exome sequencing. Genome Res 2012;22:568–76.
35. Fan Y, Xi L, Hughes DS, Zhang J, Futreal PA, Wheeler DA, et al. MuSE: accounting for tumor heterogeneity using a sample-specific error model improves sensitivity and specificity in mutation calling from sequencing data. Genome Biol 2016;17:178.
36. Kim S, Scheffler K, Halpern AL, Bekritsky MA, Noh E, Kallberg M, et al. Strelka2: fast and accurate calling of germline and somatic variants. Nat Methods 2018;15: 591–4.
37. Talevich E, Shain AH, Botton T, CNVkit BBC Genome-wide copy number detection and visualization from targeted DNA sequencing. PLoS Comput Biol 2016;12:e1004873.
38. Rausch T, Zichner T, Schlattl A, Stutz AM, Benes V, Korbel JO. DELLY: structural variant discovery by integrated paired-end and split-read analysis. Bioinformatics 2012;28:i333–i9.
39. Layer RM, Chiang C, Quinlan AR, Hall IM. LUMPY: a probabilistic framework for structural variant discovery. Genome Biol 2014;15:R84.
40. Chen X, Schulz-Trieglaff O, Shaw R, Barnes B, Schlesinger F, Kallberg M, et al. Manta: rapid detection of structural variants and indels for germline and cancer sequencing applications. Bioinformatics 2016;32:1220–2.
41. Cameron DL, Schroder J, Penington JS, Do H, Molania R, Dobrovic A, et al. GRIDSS: sensitive and specific genomic rearrangement detection using positional de Bruijn graph assembly. Genome Res 2017;27:2050–60.
42. Jeffares DC, Jolly C, Hoti M, Speed D, Shaw L, Rallis C, et al. Transient structural variations have strong effects on quantitative traits and reproductive isolation in fission yeast. Nat Commun 2017;8:14061.
43. Chiang C, Layer RM, Faust GG, Lindberg MR, Rose DB, Garrison EP, et al. SpeedSeq: ultra-fast personal genome analysis and interpretation. Nat Methods 2015;12:966–8.
44. Edgar R, Domrachev M, Lash AE. Gene Expression Omnibus: NCBI gene expression and hybridization array data repository. Nucleic Acids Res 2002; 30:207–10.
45. Bose P, Verstovsek S. JAK2 inhibitors for myeloproliferative neoplasms: what is next? Blood 2017;130:115–25.
46. Wu SC, Li LS, Kopp N, Montero J, Chapuy B, Yoda A, et al. Activity of the type II JAK2 inhibitor CHZ868 in B cell acute lymphoblastic leukemia. Cancer Cell 2015;28:29–41.
47. Das R, Guan P, Sprague L, Verbist K, Tedrick P, An QA, et al. Janus kinase inhibition lessens inflammation and ameliorates disease in murine models of hemophagocytic lymphohistiocytosis. Blood 2016;127:1666–75.
48. Kubovcakova L, Lundberg P, Grisouard J, Hao-Shen H, Romanet V, Andraos R, et al. Differential effects of hydroxyurea and INC424 on mutant allele burden and myeloproliferative phenotype in a JAK2-V617F polycythemia vera mouse model. Blood 2013;121:1188–99.
49. Verstovsek S, Mesa RA, Gotlib J, Gupta V, DiPersio JF, Catalano JV, et al. Long-term treatment with ruxolitinib for patients with myelofibrosis: 5-year update from the randomized, double-blind, placebo-controlled, phase 3 COMFORT-I trial. J Hematol Oncol 2017;10:55.
50. Jagasia M, Perales MA, Schroeder MA, Ali H, Shah NN, Chen YB, et al. Ruxolitinib for the treatment of steroid-refractory acute GVHD (REACH1): a multicenter, open-label phase 2 trial. Blood 2020;135:1739–49.
51. Quintas-Cardama A, Vaddi K, Liu P, Manshouri T, Li J, Scherle PA, et al. Preclinical characterization of the selective JAK1/2 inhibitor INCB018424: therapeutic implications for the treatment of myeloproliferative neoplasms. Blood 2010;115:3109–17.
52. Chen X, Williams WV, Sandor V, Yeleswaram S. Population pharmacokinetic analysis of orally-administered ruxolitinib (INCB018424 Phosphate) in patients with primary myelofibrosis (PMF), post-polycythemia vera myelofibrosis (PPV-MF) or post-essential thrombocythemia myelofibrosis (PET MF). J Clin Pharmacol 2013;53:721–30.
53. Shi JG, Chen X, McGee RF, Landman RR, Emm T, Lo Y, et al. The pharmacokinetics, pharmacodynamics, and safety of orally dosed INCB018424 phosphate in healthy volunteers. J Clin Pharmacol 2011;51:1644–54.
54. Evrot E, Ebel N, Romanet V, Roelli C, Andraos R, Qian Z, et al. JAK1/2 and Pan-deacetylase inhibitor combination therapy yields improved efficacy in preclinical mouse models of JAK2V617F-driven disease. Clin Cancer Res 2013;19:6230–41.
55. Soegaard SH, Rostgaard K, Skogstrand K, Wiemels JL, Schmiegelow K, Hjalgrim H. Neonatal inflammatory markers are associated with childhood B-cell precursor acute lymphoblastic leukemia. Cancer Res 2018;78:5458–63.
56. Isidro-Hernandez M, Mayado A, Casado-Garcia A, Martinez-Cano J, Palmi C, Fazio G, et al. Inhibition of inflammatory signaling in Pax5 mutant cells mitigates B-cell leukemogenesis. Sci Rep 2020;10:19189.
57. Fischer U, Yang JJ, Ikawa T, Hein D, Vicente-Duenas C, Borkhardt A, et al. Cell fate decisions: the role of transcription factors in early B-cell development and leukemia. Blood Cancer Discov 2020;1:224–33.
58. Vicente-Duenas C, Hauer J, Cobaleda C, Borkhardt A, Sanchez-Garcia I. Epigenetic priming in cancer initiation. Trends Cancer 2018;4:408–17.
59. Cobaleda C, Vicente-Duenas C, Sanchez-Garcia I. An immune window of opportunity to prevent childhood B cell leukemia. Trends Immunol 2021;42: 371–4.